Supporting Information

Cu-functionalised porous boron nitride derived from metal-organic framework

Tian Tian,[a] Jiamin Xu,[b] Ying Xiong, [a,c] Nitya Ramanan,[d] Mary Ryan,[b] Fang Xie,[b] and Camille Petit*[a]*

[a] Barrer Centre, Department of Chemical Engineering, Imperial College London, London, SW7 2AZ, UK

[b] Department of Materials and London Centre for Nanotechnology, Imperial College London, London, SW7 2AZ, UK.

[c] Departamento de Química Inorgánica, Facultad de Ciencias, Universidad Autónoma de Madrid, Campus de Cantoblanco, Madrid 28049, Spain.

[d] Diamond Light Source Ltd., Diamond House, Harwell Science and Innovation Campus, Didcot, OX11 0DE, UK.

* Corresponding author: camille.petit@imperial.ac.uk (C. Petit); tian.tian11@imperial.ac.uk (T. Tian)

1. Characterisation of Cu/ZIF-8

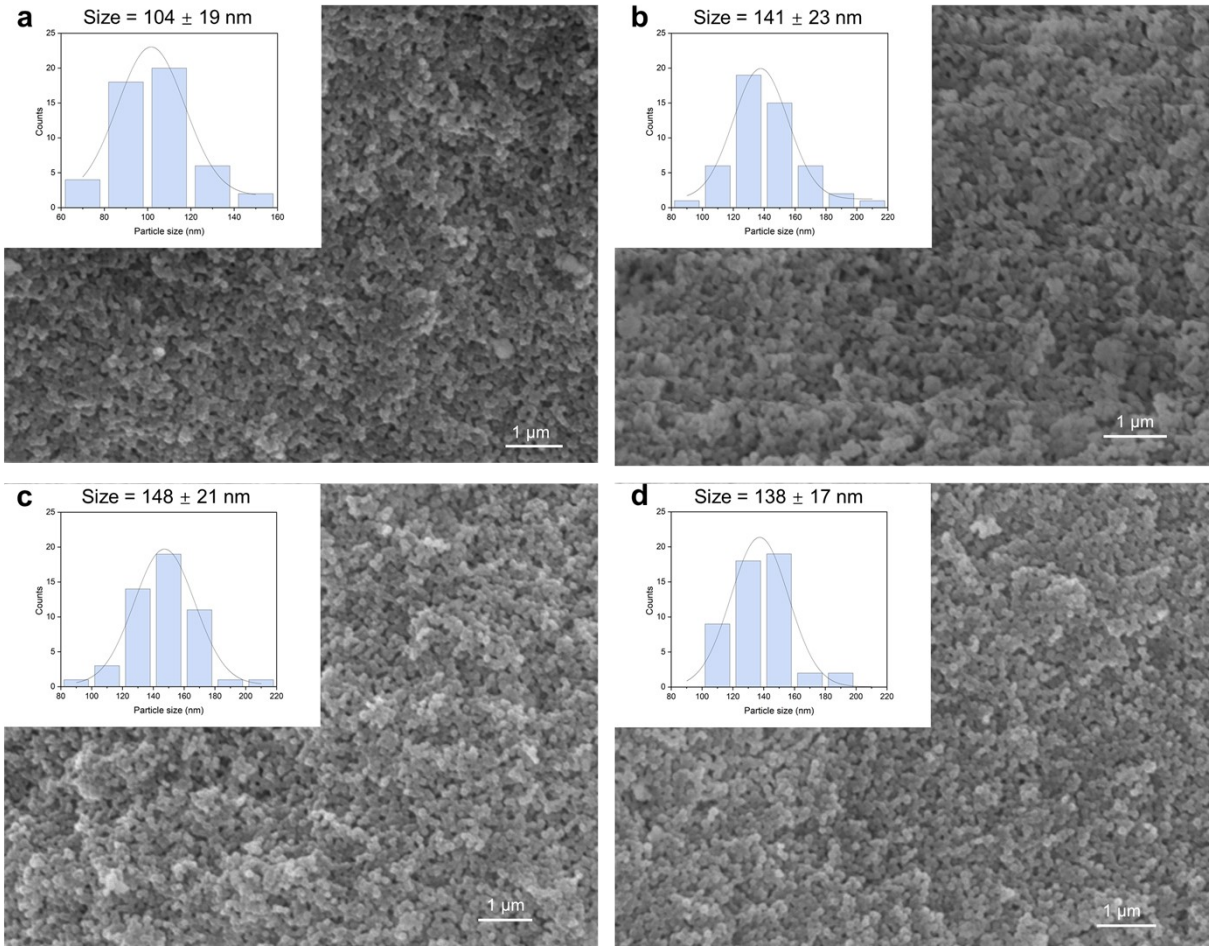

Figure S1. SEM images and primary particle size distribution of (a) ZIF-8; (b) 1% Cu/ZIF-8; (c) 5% Cu/ZIF-8; (d) 10% Cu/ZIF-8. 100 particles were randomly selected and used to measure the particle size distribution as described in the experimental section.

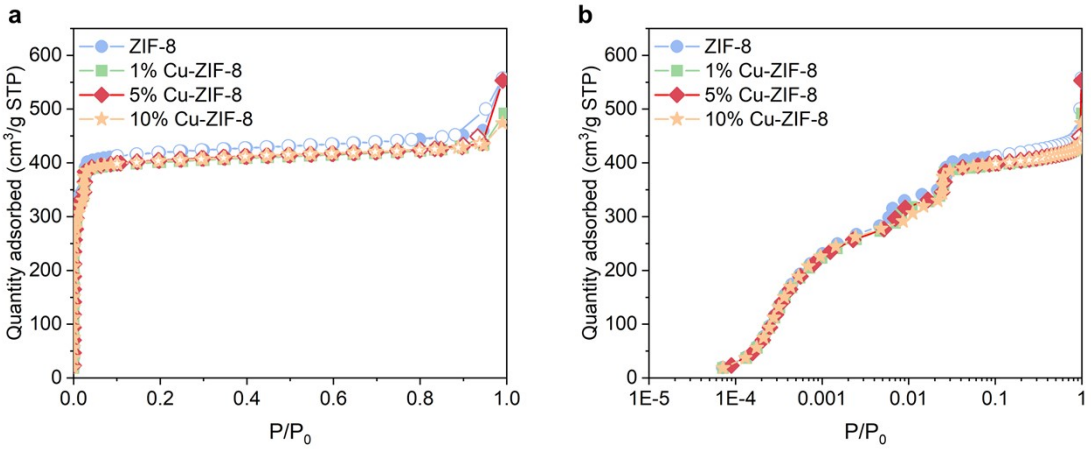

Figure S2. N_2 sorption isotherms at 77 K for Cu/ZIF-8 in (a) linear scale; (b) semi-log scale. Filled symbols: adsorption. Empty symbols: desorption.

Table S1. Textural properties of Cu/ZIF-8 samples derived from N_2 sorption isotherms at 77 K: BET area (S_{BET}), micropore volume (V_{mic}) and total pore volume (V_{tot}). The calculation methods are described in the experimental section.

	S_{BET} [m^2/g]	V_{mic} [cm^3/g]	V_{tot} [cm^3/g]
ZIF-8	1680	0.670	0.787
1% Cu/ZIF-8	1668	0.636	0.766
5% Cu/ZIF-8	1643	0.626	0.716
10% Cu/ZIF-8	1661	0.606	0.701

2. Characterisation of Cu/BN

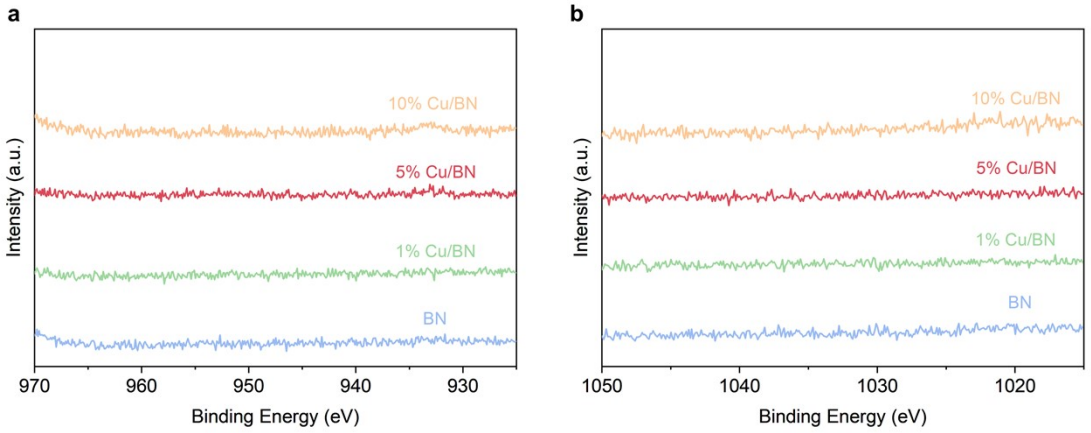

Figure S3. High resolution XPS spectra of BN and Cu/BN samples in the regions corresponding to (a) Cu 2*p* core level; (b) Zn 2*p* core level.

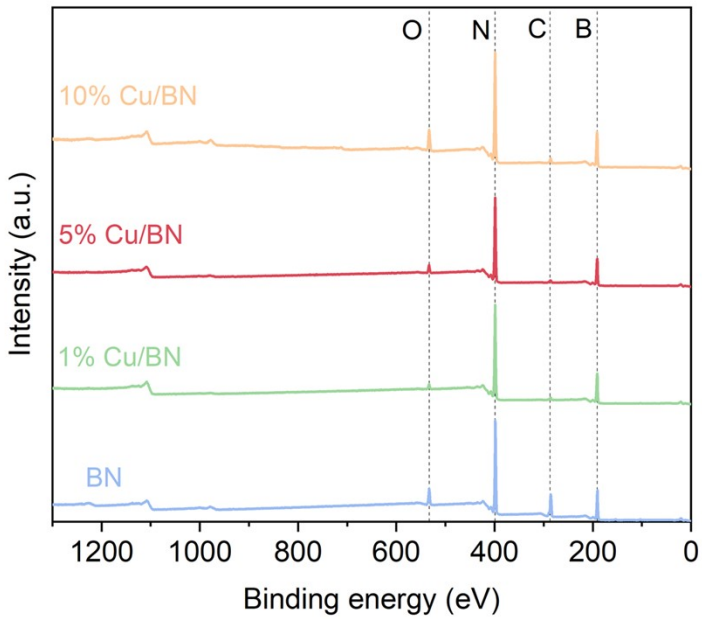

Figure S4. XPS survey spectra of BN and Cu/BN samples.

Table S2. Relative atomic composition of BN and Cu/BN samples obtained from XPS.

	B [at. %]	N [at. %]	C [at. %]	O [at. %]
BN	50.71	40.11	3.87	5.31
1% Cu/BN	51.64	41.32	2.55	4.49
5% Cu/BN	51.23	43.01	2.89	2.87
10% Cu/BN	51.27	40.00	3.46	6.27

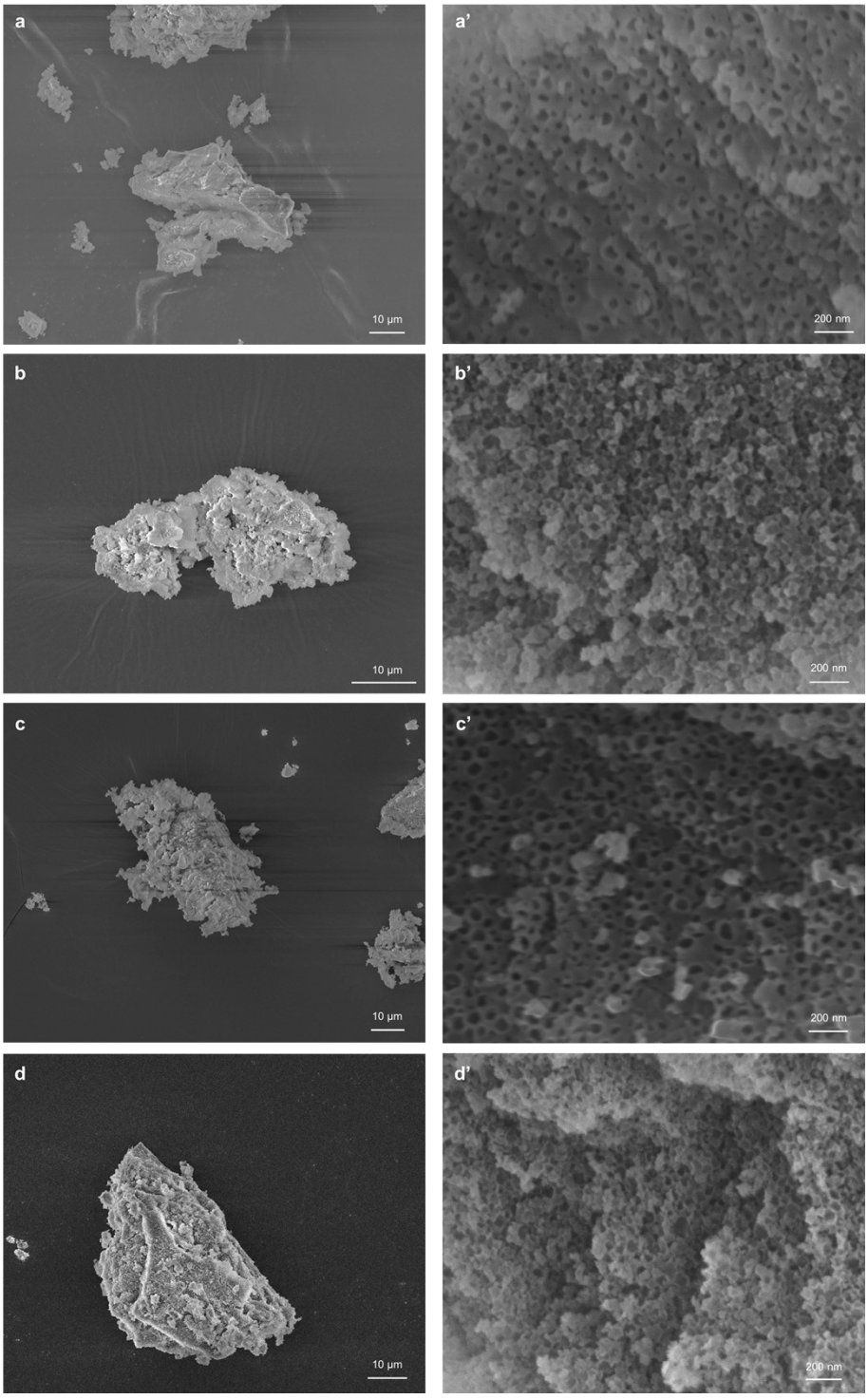

Figure S6. SEM images of (a and a') BN; (b and b') 1% Cu/BN; (c and c') 5% Cu/BN; (d and d') 10% Cu/BN.

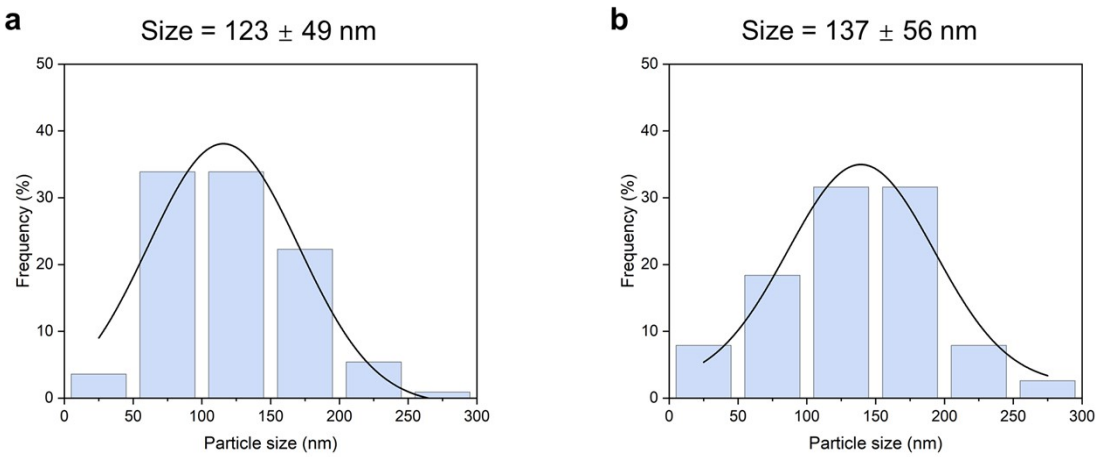

Figure S7. Particle size distribution obtained from TEM images. (a) 5% Cu/BN; (b) 10% Cu/BN. 100 Cu particles were randomly selected and used to measure the particle size distribution. The particle size distribution for the 1% Cu/BN sample is not shown here due to the limited number of Cu particles after dispersing the sample in ethanol and we could not collect enough Cu particles to calculate the size distribution.

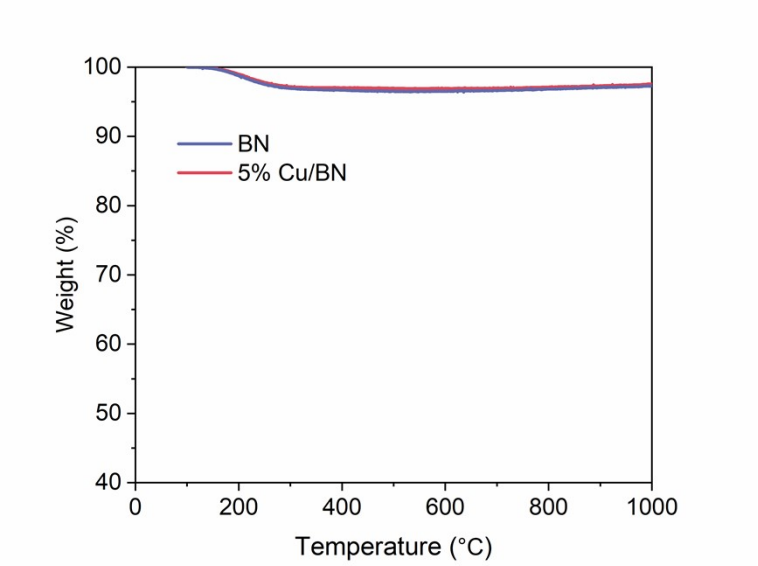

Figure S8. Thermogravimetric analysis of BN and 5% Cu/BN. The tests were performed from room temperature to 1000 °C under N_2 with a heating ramp of 5 °C/min.

3. CO_2 photoreduction testing

Normalised formation rate ($\mu mol\ e^-\ g^{-1}\ h^{-1}$)

The normalised formation rate is related to the number of reacted electrons. Two moles of electrons were required to obtain one mole of CO from CO_2 and eight moles electrons for one mole of CH_4.

Solar-to-product conversion efficiency (SPE) can be calculated by the equation:

$$\eta = \frac{n_{co} \cdot \Delta G_{co} + n_{CH_4} \cdot \Delta G_{CH_4}}{W \cdot A \cdot t}$$

Where *n* is mol of the product; ΔG_{CO} (257 kJ/mol) and ΔG_{CH4} (344 kJ/mol) are the Gibbs free energy change for the generation of one mol of CO and CH_4, respectively by reducing CO_2 under standard conditions; *W* is the intensity of the light (100 mW/cm^2), *A* is the active area (i.e. sample holder, 7 cm^2); *t* is irradiation time (5 h). The results are reported in Table S4.

Table S4. Solar-to-product efficiency (SPE) of Cu/BN compared to that of g-C_3N_4.

Sample	g-C_3N_4	BN	1% Cu/BN	5% Cu/BN	10% Cu/BN
SPE [10^{-5} %]	1.3	8.9	9.4	11.2	8.9

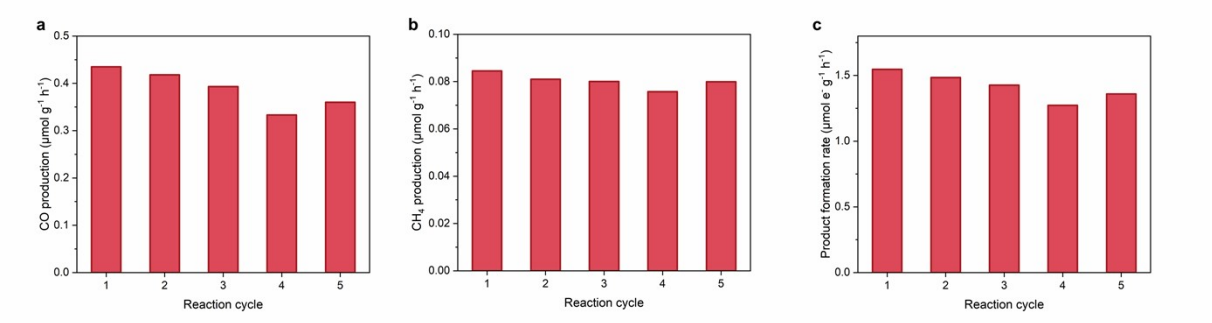

Figure S9. CO_2 photoreduction testing of 5% Cu/BN over 5 photocatalytic cycles (5 h for each cycle) under UV-Vis irradiation. (a) CO production rate; (b) CH_4 production rate; (c) normalised production rate.

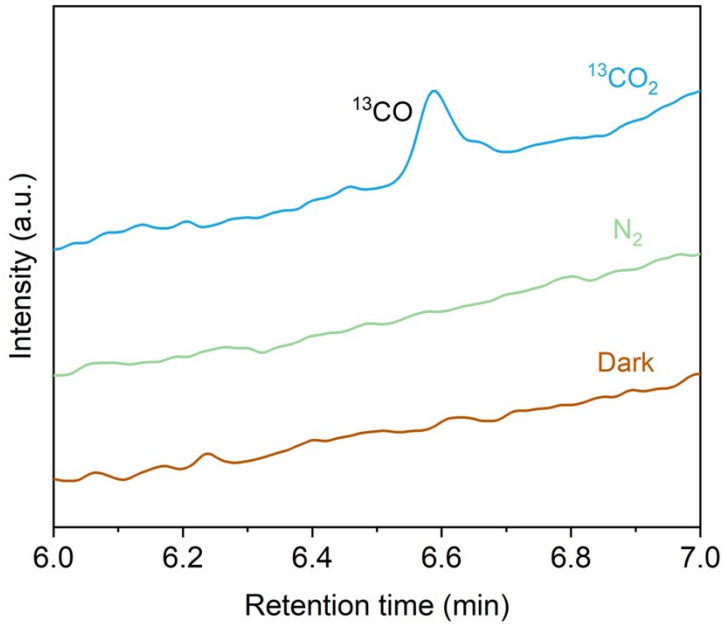

Figure S10. Gas chromatogram illustrating that under dark or N_2/H_2 atmosphere test condition, no ^{13}CO peak was observed. ^{13}CO was only observed under $^{13}CO_2/H_2$ atmosphere under light irradiation.

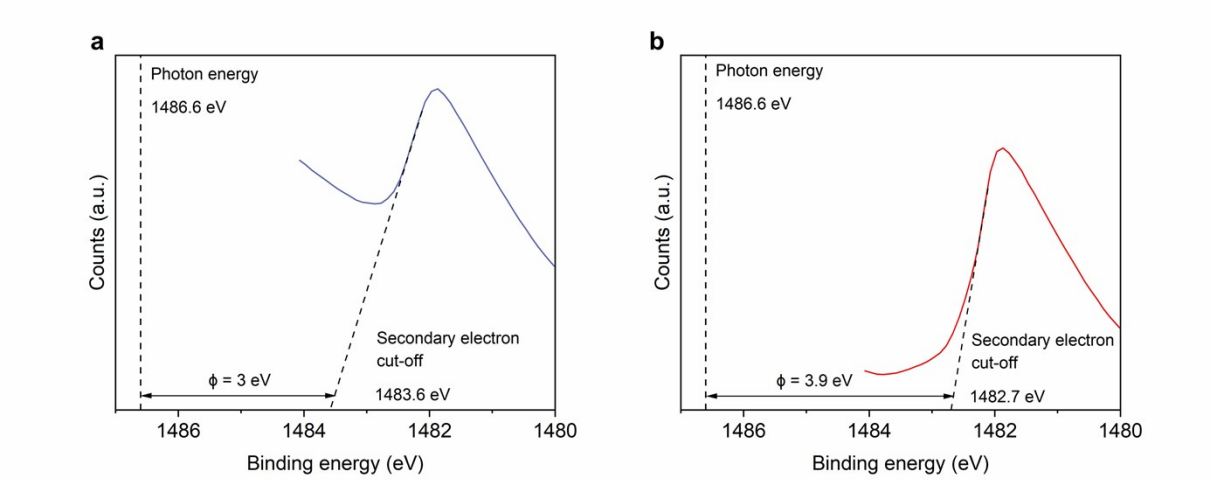

Figure S11. Secondary electron cut-off measurement through photoelectron spectroscopy. (a) BN; (b) 5% Cu/BN. The average work functions were taken over four different locations on the samples to account for potential variations across the surface.

The energy associated with the monochromatic photon source (1486.6 eV) in the XPS instrument is indicated, at which point the electrons have zero kinetic energy. The secondary electron cut-off denotes the threshold value at which the electrons have sufficient kinetic energy to overcome the work function of the sample and be detected by the spectrometer.[1,2] Extrapolating the secondary electron cut-off could obtain the work function of the material. The average work function for $_{mono}$ZIF-67 and $_{8mL}$Au@ZIF-67 is 3.00 ± 0.51 eV and 3.9 ± 0.22 eV, respectively.

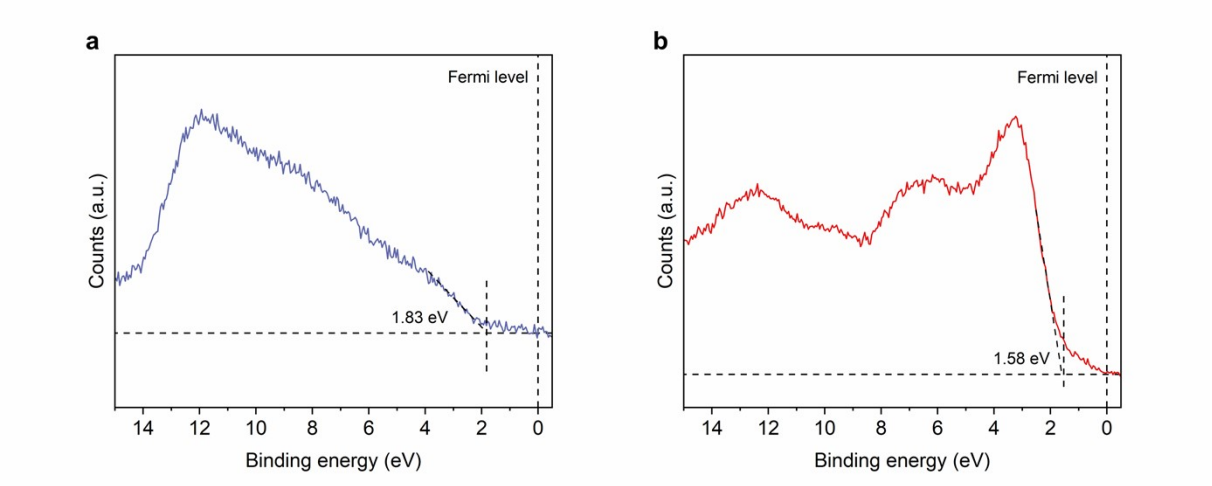

Figure S12. Valence band offset measurement to ascertain the distance between the Fermi level and valence band maximum. (a) BN; (b) 5% Cu/BN.

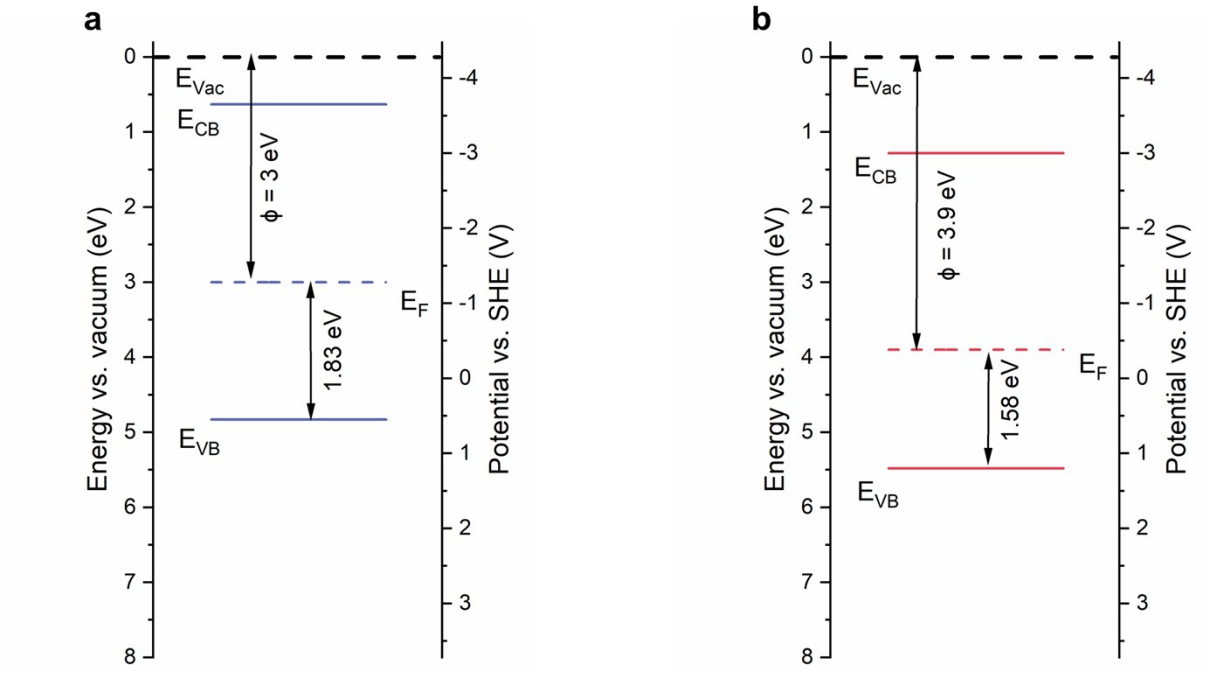

Figure S13. Band structure on the absolute energy scale vs. vacuum with the conduction (E_{CB}) and valence band (E_{VB}), Fermi level (E_F). (a) BN; (b) 5% Cu/BN.

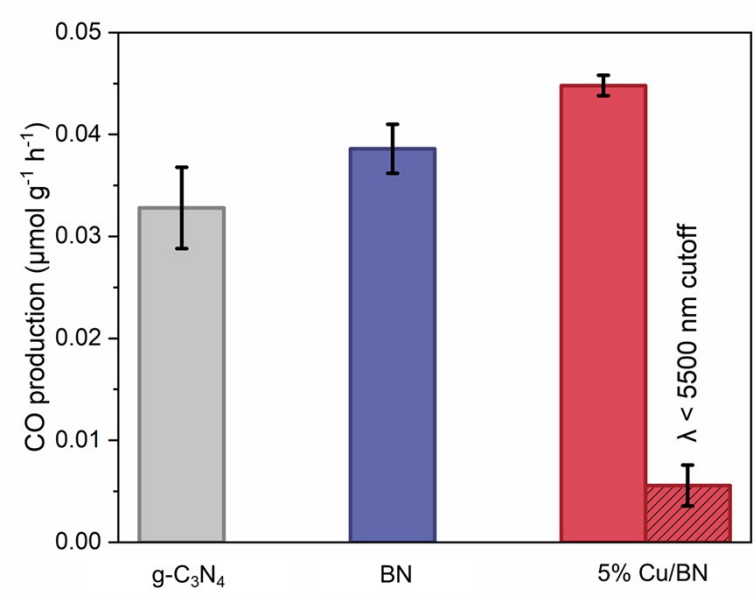

Figure S14. CO production rate under visible light (λ < 400 nm cutoff). Upon irradiation > 550 nm, g-C_3N_4 and BN did not generate any observable products. The error bars correspond to the standard deviation from 2 tests.

Porous BN can photoreduce CO_2 upon visible light irradiation owing to trap states as explained in our previous study.[3] Here, we also evaluated the visible light activity of the best-performing composite, 5% Cu/BN (Figure S14). Upon irradiation > 400 nm, 5% Cu/BN produced 37% and 15% more CO than g-C_3N_4 and pristine BN, respectively. CH_4 is not detected after 5 h irradiation. Upon irradiation > 550 nm, we did not observe any CO_2 photoreduction using pristine BN, which is consistent with our previous report.[3] However, 5% Cu/BN still produced CO, indicating the wider light absorption range upon the incorporation of Cu particles. With the characteristic plasmonic response of Cu nanoparticles, indicated in Figure 6b, the hot electrons generated by Cu nanoparticles due to the visible light absorption is the main reason for the reaction to take place.

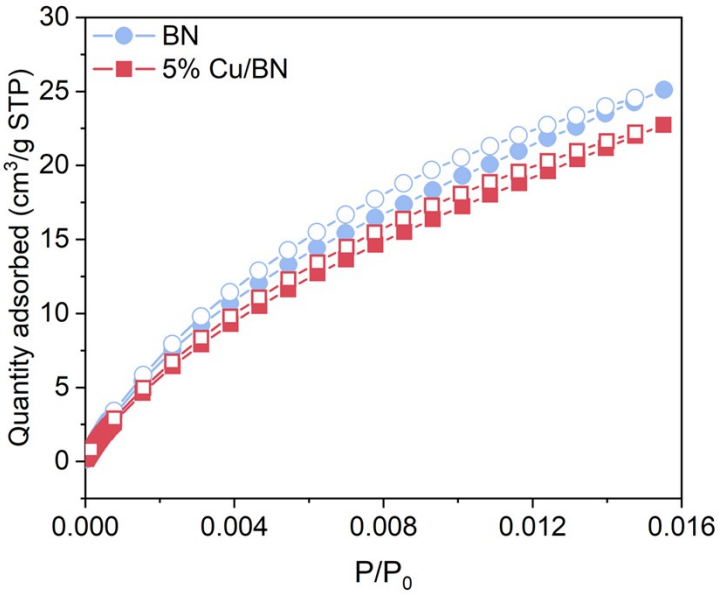

Figure S15. CO_2 sorption isotherms at 298 K for pristine BN and 5% Cu/BN. Filled symbols: adsorption, empty symbols: desorption. The results indicate the higher photocatalytic efficiency of 5% Cu/BN was not driven by the CO_2 adsorption capacity.

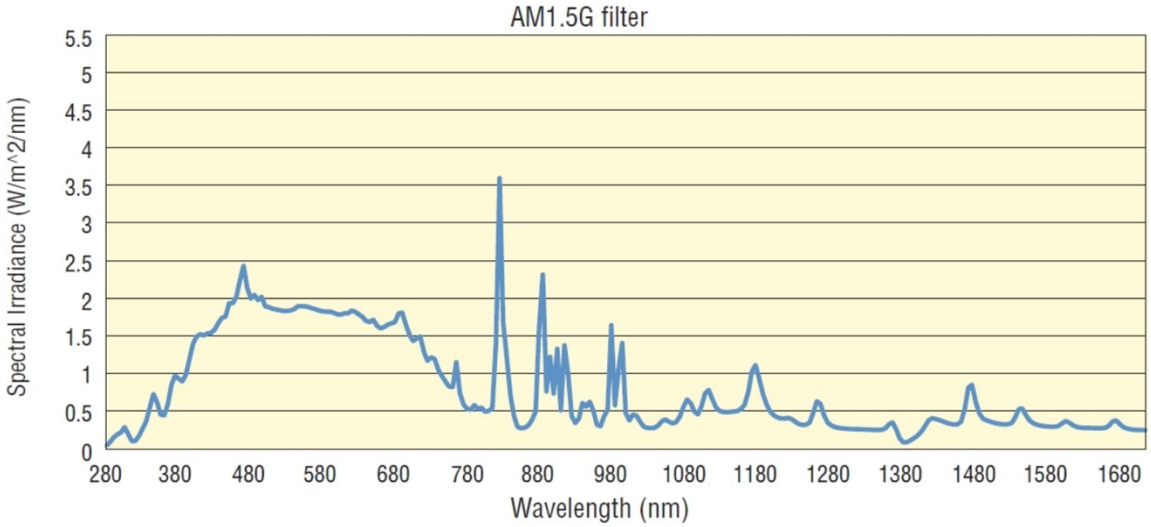

Figure S156. Spectral output of LCS-100 solar simulator with the AM1.5G filter.

4. Use of a different metal

Table S3. Relative atomic composition of samples derived from Co/ZIF-8.

	B [at. %]	N [at. %]	C [at. %]	O [at. %]
10% Co/C-BN	32.6	29.8	29.0	8.6

Table S4. Co content and textural properties of the Co/C-BN samples.

Sample	Co content [wt%]	S_{BET} [$m^2 g^{-1}$]	V_{mic} [$cm^3 g^{-1}$]	V_{tot} [$cm^3 g^{-1}$]
10% Co/C-BN	4.8	332	0.45	0.58

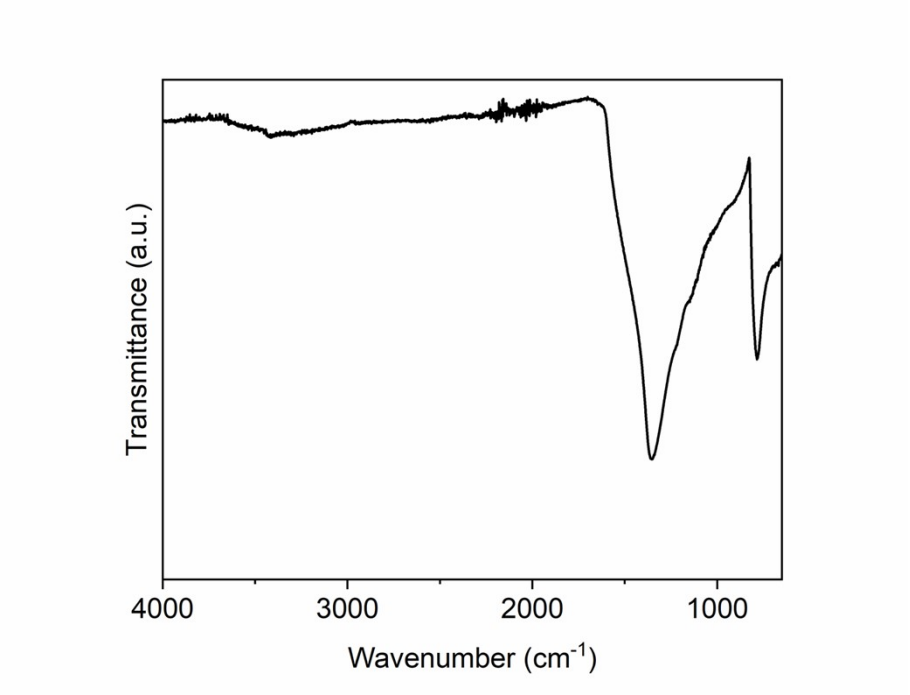

Figure S17. FTIR of 10% Co/C-BN.

References

1 R. Shankar, M. Sachs, L. Francàs, D. Lubert-Perquel, G. Kerherve, A. Regoutz and C. Petit, *J. Mater. Chem. A*, 2019, **7**, 23931–23940.

2 J. W. Kim and A. Kim, *Curr. Appl. Phys.*, 2021, **31**, 52–59.